Robotics and Computer Integrated Manufacturing 65 (2020) 101959

Contents lists available at ScienceDirect

Robotics and Computer Integrated Manufacturing

journal homepage: www.elsevier.com/locate/rcim

A point and distance constraint based 6R robot calibration method through machine vision

Rui Wang*, Anwen Wu, Xuan Chen, Jun Wang

Harbin Institute of Technology at Weihai, Weihai 264200, China

ARTICLE INFO

Keywords:
Kinematic calibration
Machine vision
Point constraint
Distance constraint

ABSTRACT

This paper proposes a 6R robot closed-loop kinematic calibration method to improve absolute position accuracy with point and distance constraints though machine vision. In the calibration process, a camera attached to the mounting plate of the robot is used to capture a fixed reference sphere as a point constraint and to record robot joint angles and gauge block lengths that are used as a distance constraint. A first-order difference quotient is used to calculate the Jacobian matrix in the joint parameter identification process. The Staübli TX60 robot is successfully calibrated using the proposed method. After calibration, the average distance error of robot motion is decreased from 2.05 mm to 0.24 mm.

1. Introduction

In current manufacturing processes, robots are required to perform not only simple motions but also complex trajectory movement, continuous contact operation to achieve flexible production of small batches or multi-varieties [1] and multi-robot cooperative work [2]. These tasks are difficult for industrial robots with high repetitive positioning accuracy, but poor absolute positioning accuracy. Robot part errors in manufacturing and assembly, creepage in continuous high load conditions, collision and so on will lead to deviations between the actual kinematic parameters and nominal ones [3]. These deviations are called kinematic errors and will result in absolute positioning errors of the robot end effector (EE). An obvious manifestation is that when the robot reaches the same nominal position with different joint configuration, the actual position of the end effector is changed significantly. A specific pose of the 6R robot EE has several different joint configurations which correspond to multiple solutions of the robot inverse solution.

Regarding off-line programming, robots should satisfy high absolute position accuracy. Among the factors that affect the overall accuracy of the robot, errors caused by small deviation in kinematic parameters accounts for approximately 80% of the total errors [4]. Therefore, kinematic calibration is an effective method to improve the absolute positioning accuracy of the robot when the repetitive positioning accuracy of the robot is sufficient [5]. Many scholars have provided calibration methods.

Robot calibration methods are divided into open-loop calibration and closed-loop calibration [6]. Tang and Mooring [7] utilized a special fixture consisting of a plate with accurately located points to obtain the partial pose information of a robot EE and performed a calibration process. After calibration, the maximum error of the PUMA560 was reduced from 2.5 mm to 0.45 mm, and the average error was reduced from 0.715 mm to 0.197 mm. Ahmed Joubair and Ilian A. Bonev [8] built a plane constraint by maintaining contact between a fixed granite plate and a touch probe settled on the robot EE. After calibration, the maximum distance error of the FANUC LR Mate 200iC series robot was reduced from 1.321 mm to 0.274 mm. However, the robot EE error acquisition procedure of these two methods is time consuming.

Du and Zhang [9] proposed an on-line calibration method based on machine vision. A camera settled on the robot EE was used to automatically capture a fixed chessboard at different angles and to inversely determine the robot pose by extracting the chessboard corner points. A robot grasping experiment was performed to verify the proposed calibration method result. After calibration, the mean absolute position errors decreased from 5.62, 6.85, and 7.33 mm to 1.22, 1.34, and 1.53 mm. This method has a high degree of automation but requires a high-performance camera with automatic zoom, extended depth of field and minor distortion functions.

Wang [10] proposed a closed-loop calibration method based on a plane constraint and contact measuring probe with an auxiliary camera to improve measurement efficiency. The measuring accuracy of the probe was within 0.030 mm, while the average error of the robot was reduced from 1.266 mm before calibration to 0.562 mm after calibration. However, this method relies on expensive equipment and is

* Corresponding author.
E-mail addresses: wrhit@163.com (R. Wang), 1261288097@qq.com (X. Chen).

https://doi.org/10.1016/j.rcim.2020.101959
Received 30 April 2019; Received in revised form 9 November 2019; Accepted 9 February 2020
Available online 11 March 2020

difficult to popularize.

Beyer and Wulfsberg [11] proposed a machine vision-based calibration method by using a special tool which is consist of two cameras and a fixed reference sphere to record the deviations of sphere position at different tool pose in three dimensions. The medium error of KUKA KR45 after calibration is decreased from 1.44 mm to 0.12 mm. This method relies on very good lenses optical quality and high fixture accuracy to ensure the coincidence of theoretical and practical relative position of the two camera optical axles.

From other calibration literature [12–18] open-loop calibration is known to easily identify robot joint parameters and lead to better calibration results, but the related equipment is bulky and expensive.. Conversely, the parameter identification process in closed-loop calibration is difficult, but the measurement devices used are economical and convenient. The major disadvantages of most closed-loop calibration methods are the amount of time consumed or low accuracy.

Currently, closed-loop calibration methods are not widely used. Several robot manufacturers or other institutions provide a one-time open-loop calibration service. However, this is only appropriate for customers with one or few robots and the deployment of measuring equipment in complex factory environments is difficult and time consuming. A cost-effective closed-loop calibration method has great potential for promotion.

In Section 2, we introduce the robot kinematic model. In Section 3, we present the measurement process and simulation measurement experiment. In Section 4, we present the calibration method and parameter identification method. In Section 5, we present the calibration experiment of TX60. In Section 6, we present the conclusions.

2. Robot model

2.1. Kinematic model

The robot used in this paper is the Staübli 6R robot TX60 as shown in Fig. 1. The repetitive positioning error is within 0.02 mm. Similar to other robotic manipulators, the absolute positioning accuracy is not mentioned in the product manual.

As shown in Eq. (1). the MDH model [19] is built on the robot with joint parameter deviations. Each joint has a useless joint parameter (the bold zero in Table 1). Parameter d is zero for adjacent parallel joints, and β is zero for other joints.

$$ {}_{i}^{i-1}\boldsymbol{T} = Rot(z_{i-1}, \theta_i)Trans(z_{i-1}, d_i)Trans(x_i, a_i)Rot(x_i, \alpha_i)Rot(y_i, \beta_i) \tag{1} $$

Among the parameters in Table 1 d_1 and θ_1 can be transformed to the joint parameters of robot mounting base, and calibrated separately after the robot is installed. The parameters for joint 7 represent the nominal transformation from the robot flange coordinate system to an intermediate coordinate system whose axes are parallel to the camera coordinate axes and whose origin is at the intersection of the camera optical axis and the flange plane. Joint 6 is rigid coupled with and can be considered part of joint 7, as shown in Fig. 1. Parameter deviations of joint 6 are skipped and included in tool parameter deviations. Tool calibration is not the focus of this paper and most robot manufacturers provide this function. The 22 unmarked joint parameters in Table 1 are the parameters to be calibrated and are recorded as vector ***JP***.

2.2. Inverse solution

The inverse solution based on the parameters that describe the physical robot kinematics exactly needs to be solved iteratively with the inverse solution based on nominal joint parameters as the initial value. The following inverse solution means the actual parameter based inverse solution process. Inverse solution is used in simulation measurement and result verification after the calibration experiment.

$$ \boldsymbol{J_I} = [\boldsymbol{J_{I1}} \ \cdots \ \boldsymbol{J_{Ij}} \ \cdots \ \boldsymbol{J_{I6}}] = \begin{bmatrix} a_{11} & \cdots & a_{16} \\ \vdots & \ddots & \vdots \\ a_{61} & \cdots & a_{66} \end{bmatrix} \tag{2} $$

$$ \begin{aligned} \boldsymbol{JA_{d1}} &= [1^{\circ} \ 0 \ 0 \ 0 \ 0 \ 0]^T \\ \boldsymbol{JA_{d2}} &= [0 \ 1^{\circ} \ 0 \ 0 \ 0 \ 0]^T \\ &\cdots \\ \boldsymbol{JA_{d6}} &= [0 \ 0 \ 0 \ 0 \ 0 \ 1^{\circ}]^T \end{aligned} \tag{3} $$

$$ \boldsymbol{T} = \begin{bmatrix} \boldsymbol{R} & \boldsymbol{P} \\ 0 & 1 \end{bmatrix} = \begin{bmatrix} \boldsymbol{n} & \boldsymbol{o} & \boldsymbol{a} & \boldsymbol{P} \\ 0 & 0 & 0 & 1 \end{bmatrix} = \begin{bmatrix} n_x & o_x & a_x & P_x \\ n_y & o_y & a_y & P_y \\ n_z & o_z & a_z & P_z \\ 0 & 0 & 0 & 1 \end{bmatrix} \tag{4} $$

The effect matrix of each joint angle on the end position and pose is Jacobian matrix, recorded as $\boldsymbol{J_I}$. a_{ij} in Eq. (2) is the influence coefficient of the jth joint angle on the ith value of the end position and pose. The inverse solution, which has six degrees of freedom, is unique when the joint configuration is specified, so the Jacobian matrix is invertible for the 6R robot. The inverse solution progress is shown in **Fig. 2** ***C*** is the position and pose vector in Cartesian form $((x, y, z, rx, ry, rz)^T)$. $\boldsymbol{C}_t$ is the target value of the EE position and pose. ***JA*** is the joint angle vector. ***JP*** is the joint parameter vector. The forward solution function used to obtain the Cartesian position and pose of the EE is recorded as $F_{FC}(\boldsymbol{JA}, \boldsymbol{JP})$. The F in the subscript represents the forward solution and the C represents the result recorded in Cartesian form. If C is replaced by T, that means the result is recorded in the transformation matrix form shown in Eq. (4). The joint angles of TX60 can be solved quickly and accurately at a certain pose and position in its workspace using the above method.

3. Measurement process and simulation measurement

3.1. Measurement and calibration method

This paper proposed a point and distance constraint based 6R robot calibration method. The simulation experiment results show that the point constraint calibration method has low accuracy in identification of length parameters of joint 2 and 4. A distance constraint method is developed as a supplement to improve the identification accuracy of these two joints. The point constraint is built by driving TX60 EE to a certain position in a different pose and recording the joint angles when this pose-change motion is settled. The joint angles are used to calculate the EE pose and position, which is based on the nominal joint parameters. A distance constraint is built by driving TX60 EE to two points whose spacing is known and recording joint angles separately. Those joint angles are used to calculate the distance between two EE positions, which is based on the nominal joint parameters. If the joint parameters used are not coincident with the actual parameters, the calculated EE position and distance will not coincide with the actual position and distance.

3.2. Measurement tool

The reference sphere used in this paper is a ceramic ball with high sphericity, and a diameter of 25.4 mm. The GT3400 camera with manual zoom and a resolution of 3384 × 2704 is used. Imaging of the sphere is performed at the center of the camera's field of view to minimize the effect of radial distortion, which means the sphere is on the optical axis of the camera. The relative position of the sphere center to the camera is acquired by image processing.

3.3. Point constraint measurement

The point constraint is measured as follows. First, the camera is attached to the EE of the TX60. Then, the camera is used to capture the

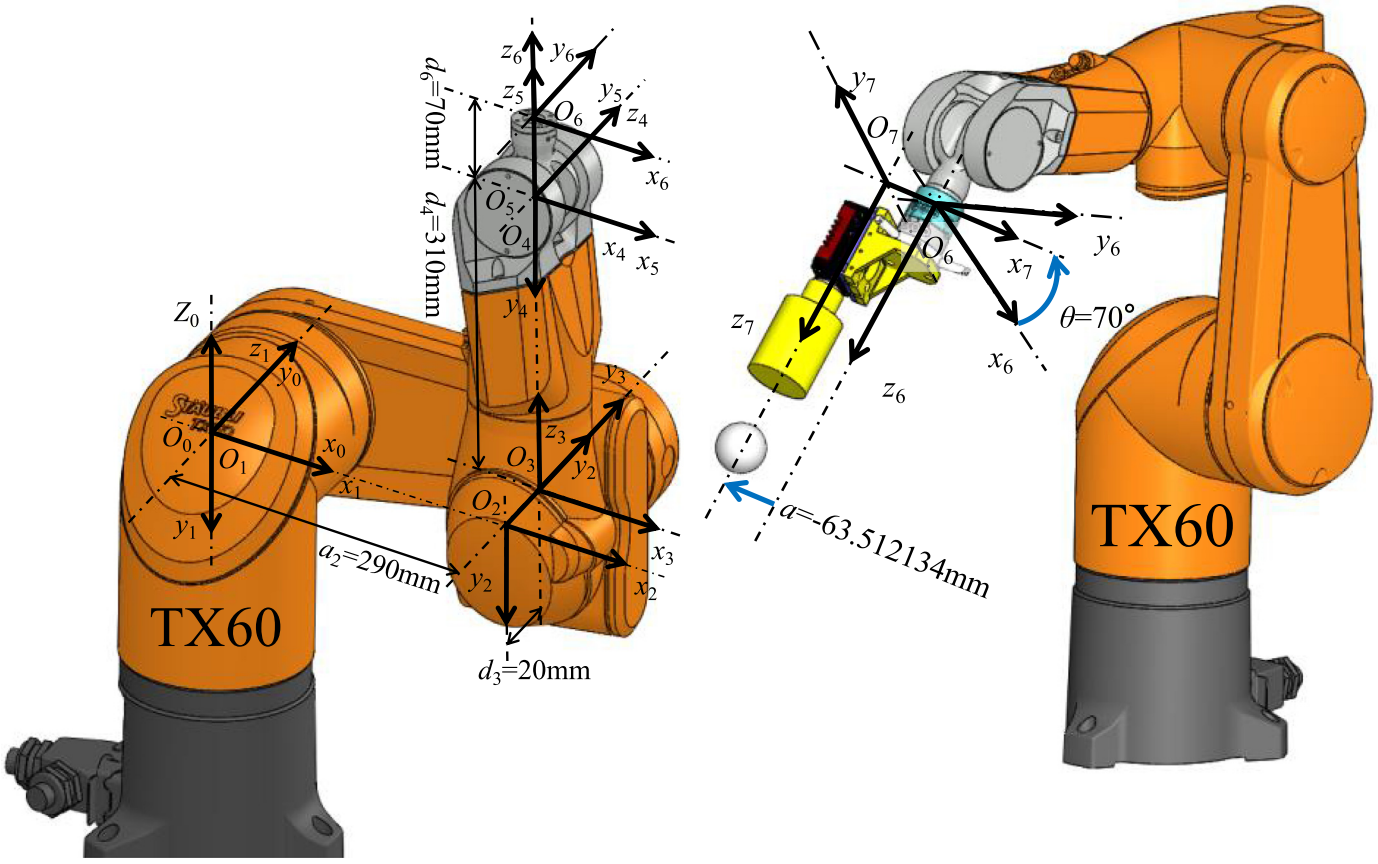

Fig. 1. 3D model and joint model of TX60 and camera module.

Table 1
Theoretical kinematic joint parameters of TX60.

Joint i	θ(°)	d(mm)	a(mm)	α(°)	β(°)
1	0	0	0	−90	**0**
2	−90	**0**	290	0	0
3	90	20	0	90	**0**
4	0	310	0	−90	**0**
5	0	0	0	90	**0**
6	–	70	–	–	**0**
7	70	0	−63.5121	0	0

fixed sphere from different angles, the camera position is adjusted to position the sphere in the center of the image and maintain a certain distance between the sphere and camera so that the sphere image is the same size. Finally, the robot joint angles are recorded separately when the angle-change motion is completed. While keeping the sphere in the same position, the camera optical axis at different poses are supposed to intersect at a point, which is the center of the sphere, as shown in Fig. 3. The actual measurement is shown in Fig. 4. In the measured point constraint data, the joint angles are recorded as the vector $\boldsymbol{JA}_p$. The coordinates of the sphere in the camera coordinate system are recorded as vector $\boldsymbol{\Delta P}_{pc}$, which is called centering error and obtained by image processing. The unknown actual sphere coordinates in the robot basal coordinate system are marked as vector $\boldsymbol{P}_{Bp}$.

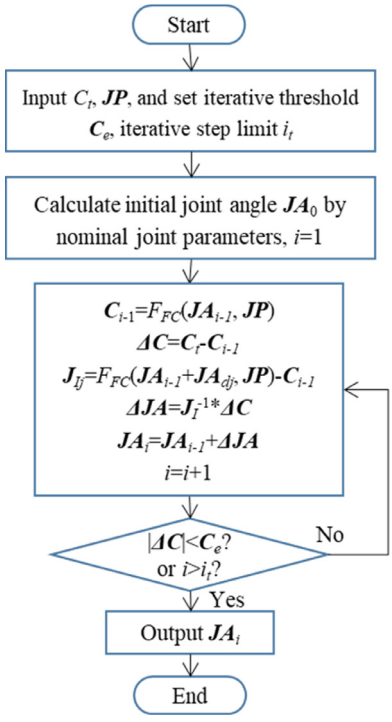

Fig. 2. Inverse solution flow-chart.

3.4. Distance constraint measurement

The distance constraint measurement process is as followed. First, the sphere is placed at two positions in sequence with several gauge blocks in between, which means the distance of the two positions is known, as shown in Fig. 5. Then, the sphere is captured at the same camera angle, and the sphere is maintained in the center of the camera field of view. Finally, the joint angles and gauge block length is recorded. Since the distance between the camera and the sphere center is difficult to measure and has repetitive error, it is necessary to ensure the

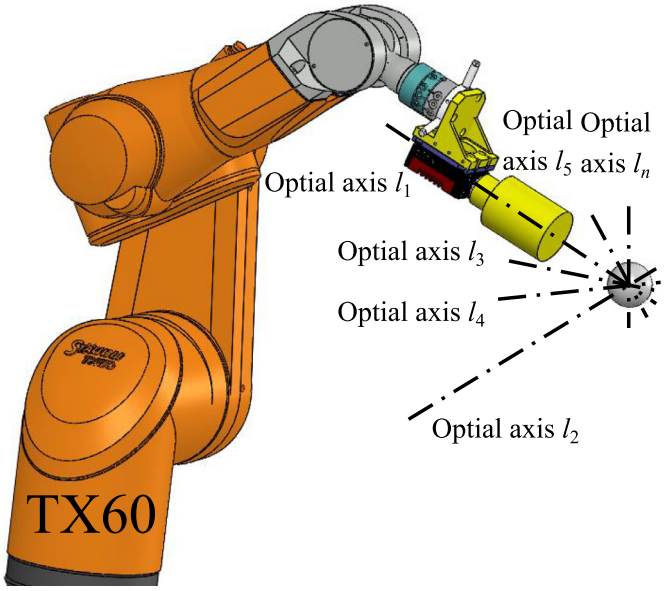

Fig. 3. Point constraint calibration 3D schematic diagram.

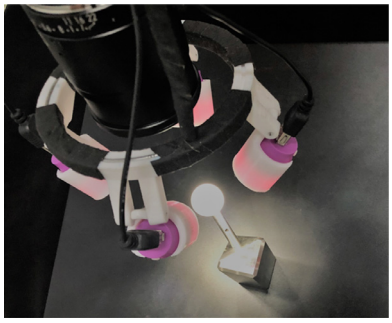

Fig. 4. Point constraint measurement.

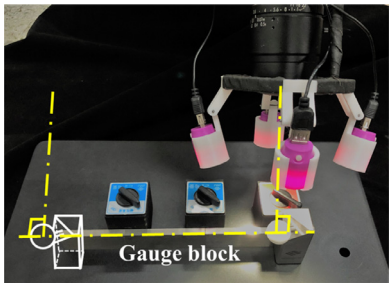

Fig. 5. Distance constraint measurement.

camera poses remain as unchanged as possible and the optical axes are kept perpendicular to the line of the two sphere centers. In the measured distance constraint data, the joint angles are recorded as vector $\boldsymbol{JA}_d$. The coordinates of the sphere in the camera coordinate system are recorded as vector $\Delta\boldsymbol{P}_{dc}$. The unknown actual sphere coordinates in the robot basal coordinate system are recorded as vector $\boldsymbol{P}_{Bd}$. The actual measured distance between the two spheres are recorded as vector d_B.

3.5. Image processing

The sphere center coordinates in the image coordinate system are obtained by fitting the edge of the sphere image and transformed to the camera coordinate system, as shown in Fig. 6. Since the sphere is close to the camera, the side of the sphere, which corresponds to the outer sphere edge in the image, requires a sufficient amount of light. The

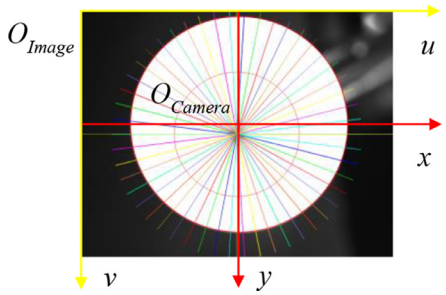

Fig. 6. Fitting the sphere edge and determining the sphere center coordinates in image coordinate system then transfer to the camera coordinate system.

centering motion would be automatically performed with real-time image feedback. Compared to the method of Du and Zhang [8] the error of this method is within 0.02 mm due to the high sphericity of the ceramic sphere.

3.6. Simulation measurement

The simulation measurement is designed to verify the practicability of the calibration method and is a simpler method than the actual measurement process. First, set the joint parameters, sphere positions, camera pose and so on. Then, calculate the corresponding joint angle using the inverse solution method previously mentioned. Random errors are added to the simulation process to simulate actual measurement errors.

4. Parameter identification

4.1. Point constraint identification process

$F_{7FC}(\boldsymbol{JA}, \boldsymbol{JP})$ is a forward solution function of the camera coordinate system. In the subscript, 7 indicates that the solution contains camera module, F and C has the same meaning as in $F_{FC}(\boldsymbol{JA}, \boldsymbol{JP})$. The point constraint equation is shown in Eq. (5).

$$F_{7FT}(\boldsymbol{JA_P}, \boldsymbol{JP_a})\cdot\Delta\boldsymbol{P_{pc}} = \boldsymbol{P_{Bp}} \tag{5}$$

The point constraint equation only considers x, y coordinates. The z coordinates, which indicate the distance between the sphere center and camera, are not included. T() is the function used to transform the three-dimensional homogeneous coordinates vector into the transformation matrix. Then, the Eq. (5). is transformed into Eq. (6).

$$(F_{7FT}(\boldsymbol{JA_p}, \boldsymbol{JP_a})\cdot\boldsymbol{T}(\Delta\boldsymbol{P_{pc}}))^{-1}\cdot\boldsymbol{P_{Bp}} = \begin{bmatrix}0\\0\end{bmatrix} \tag{6}$$

Eq. (6). only holds when the joint parameters $\boldsymbol{JP}$ are equal to the actual values $\boldsymbol{JP}_a$. Otherwise, the z axis of the camera coordinate system obtained by the forward solution is not coincident with the sphere center, and the x and y coordinates of the sphere in the camera coordinate system are recorded as $\boldsymbol{\Delta P}_{pcx}$ and $\boldsymbol{\Delta P}_{pcy}$.

The accurate sphere position $\boldsymbol{P}_{Bp}$ is unknown and replaced by the common perpendicular line's midpoint of the first two measurement optical axes, which is recorded as $\boldsymbol{P}_{Bp}'$, in the parameter identification process, as shown in Fig. 7. Then, Eq. (6) is transformed into Eq. (7). The left side of Eq. (7) is the deviation between the sphere center and the current joint parameters.

$$\begin{bmatrix}\Delta P_{pcx}\\ \Delta P_{pcy}\end{bmatrix} = (F_{7FT}(\boldsymbol{JA_p}, \boldsymbol{JP})\cdot\boldsymbol{T}(\Delta\boldsymbol{P_{pc}}))^{-1}\cdot\boldsymbol{P_{Bp}}' \tag{7}$$

The parameter identification equation is shown in Eq. (8). $\boldsymbol{J}_C$ is Jacobian matrix, where the $(2i, j)$ element represents the influence coefficient of the jth joint parameter on the ith sphere coordinates deviation on the X axis. C in $\boldsymbol{J}_C$ stands for calibration. Vector $\Delta\boldsymbol{JP}$ are the

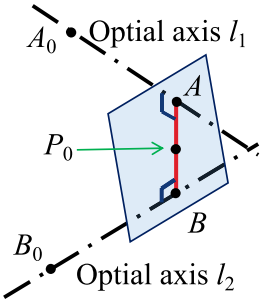

Fig. 7. Common perpendicular line's midpoint of two optical axes.

joint parameters to be adjusted. The right side of Eq. (8) is the calculated sphere coordinate deviation. Due to the complexity of the identification equations and to avoid the heavy computational burden of differential transformation, which is commonly used in calibration studies, the Jacobian matrix is calculated by the first-order difference quotient used in the inverse solution.

$$\boldsymbol{J}_{\mathrm{C}}\cdot\Delta\boldsymbol{JP}=\begin{bmatrix}\Delta P_{pcx1}\\ \Delta P_{pcy1}\\ \Delta P_{pcx2}\\ \vdots\end{bmatrix} \tag{8}$$

$\Delta\boldsymbol{JP}$ in Eq. (8) can be solved by Levenberg-Marquardt algorithm [20] or QR decomposition method. During the solution process, $\Delta\boldsymbol{JP}$ converges to a special solution when parameter identification based on point-constrained measurement data with fixed focal length is used. The length parameters of the joints in this special solution are close to zero, i.e., the origin of the camera coordinate system and the sphere center all converge on the origin of the robot basal coordinate system, as shown in Fig. 8. Therefore, it is necessary to limit the solution range.

While the calibration method based on a point constraint would only lead to large errors of the 5th and 7th joint parameters due to high coupling among parameters, the sphere center coordinates calculated using the forward solution based on identified joint parameters are very close to the preset coordinates, but the deviation of camera pose is large. Using a variable focal length in the measurement process will constrain the optical axis and improve the identification results. In the simulation measurement and identification process, with measurement error omitted, the deviation between identification results and preset joint parameters is shown in Fig. 9 which contains the fixed focal length method and changed focal length method.

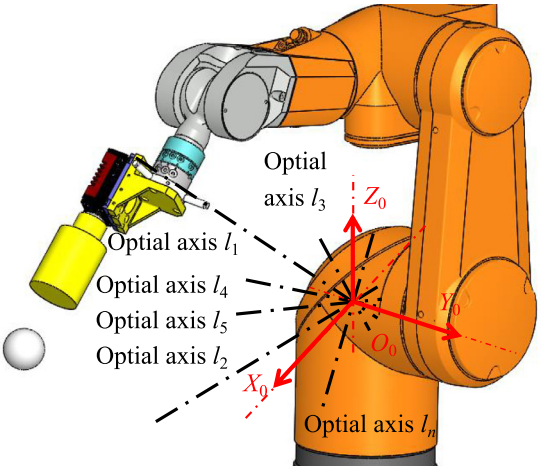

Fig. 8. Special solution in point constraint calibration without a limited range.

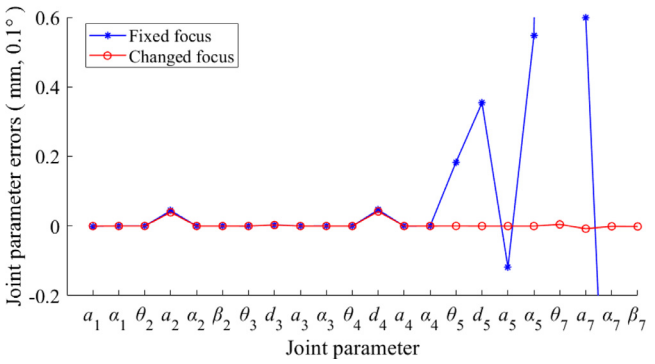

Fig. 9. Simulation identification errors of fixed focus and changed focus.

4.2. Point constraint measurement and measurement errors

The centering error of the experiment equipment is within 0.02 mm and centering deviations $\boldsymbol{\Delta P}_{pc}$ and $\boldsymbol{\Delta P}_{dc}$ obtained through image processing improved the centering accuracy to some extent but cannot eliminate errors. During simulation calibration, measurement errors were found to significantly influence the calibration results when the calibration process was only based on point constraint measurement data. The deviation between identification results and preset joint parameters is shown in Fig. 10. In the figure, σ is the standard deviation of normally distributed measurement errors. Those errors are added to the sphere coordinates in the simulation measurement process. The error mathematical expectation μ is 0.

The point constraint calibration errors are mainly focused on a_2 and d_4, and these errors are approximately proportional to their ideal value. If described as vectors, there are three main vectors from the robot basal coordinate system origin to the sphere center. Proportional variation of a_2 and d_4 to the nominal length leads to variation of the calculated sphere center, but the calculated camera optical axes at different poses will still converge at this sphere center, as shown in Fig. 11.

4.3. Distance constraint identification process

Combined with the point constraint measurement, a distance constraint calibration is proposed as a supplement to improve the identification accuracy of joint length parameters (mainly for a_2 and d_4). The distance constraint calibration process is similar to the point constraint process. Eq. (9) is the distance constraint equation, which is transformed into Eq. (10) to facilitate iterative computation. The combined equation of point constraint and distance constraint is Eq. (11).

$$|F_{7FT}(\boldsymbol{JA_{d1}},\boldsymbol{JP_a})\cdot\boldsymbol{\Delta P_{dc1}}-F_{7FT}(\boldsymbol{JA_{d2}},\boldsymbol{JP_a})\cdot\boldsymbol{\Delta P_{dc2}}|=d_B \tag{9}$$

$$\Delta d_B=d_B-|F_{7FT}(\boldsymbol{JA_{d1}},\boldsymbol{JP})\cdot\boldsymbol{\Delta P_{dc1}}-F_{7FT}(\boldsymbol{JA_{d2}},\boldsymbol{JP})\cdot\boldsymbol{\Delta P_{dc2}}| \tag{10}$$

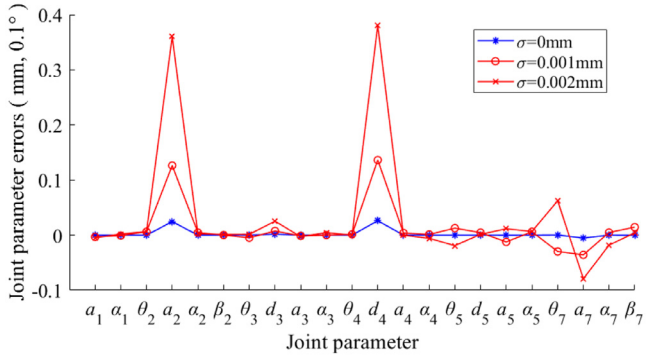

Fig. 10. Deviation between identified joint parameters and preset parameters for different distributed measurement errors based on point constraint.

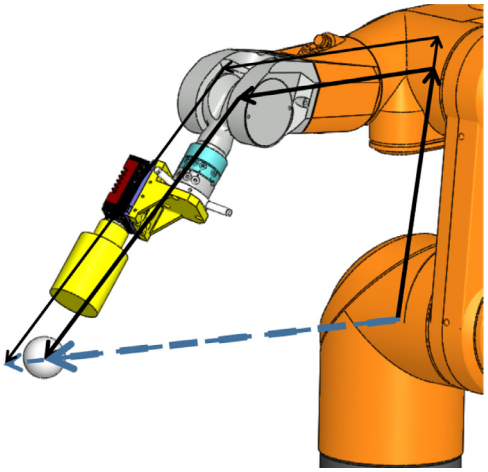

Fig. 11. Vector variations from the robot coordinate system origin to the sphere center.

$$\boldsymbol{J}_C \cdot \boldsymbol{\Delta JP} = \begin{bmatrix} \Delta P_{pcx1} \\ \Delta P_{pcy1} \\ \Delta P_{pcx2} \\ \vdots \\ \Delta d_{B1} \\ \Delta d_{B2} \\ \vdots \end{bmatrix} \tag{11}$$

The absolute deviation between identified parameters and preset joint parameters in the simulation calibration is shown in Fig. 12. The preset centering deviations obey a $N(0, 0.02^2)$ distribution. The measurement errors obey $N(0, \sigma^2)$. From the diagram, the measurement errors have lesser influence on the combined calibration method, and the measurement errors have lesser influence on the identification results. Therefore, the calibration method adopted is based on point and distance constraints. In the point constrain calibration, two different focal lengths at each sphere position are used to achieve the centering motion.

5. Calibration experiment

In the calibration experiment of Staübli TX60 robot, after eliminating measurement data with large errors, there are 202 remaining sets of data that contain point constraint measurement data of four sphere positions and 10 sets of distance constraint measurement data. Each centering motion is repeated 3 times to reduce the measurement error. The parameter identification results are shown in Table 2.

The nominal joint parameters are replaced with identified joint

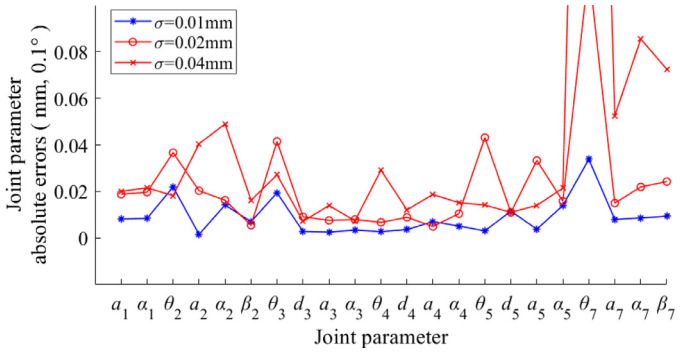

Fig. 12. Deviation between identified joint parameters and preset joint parameters for different distributed measurement errors based on combined constraint.

Table 2
Compensation values of TX60 joint parameters after Calibration.

Joint i	θ(°)	d(mm)	a(mm)	α(°)	β(°)
1	–	–	−0.0451	0.02032	–
2	0.01482	–	−0.2982	0.00536	−0.0014
3	−0.06474	0.1867	0.0538	0.01461	–
4	0.26701	−0.7793	−0.0647	−0.00406	–
5	0.44495	0.1481	0.0285	0.02675	–

parameters to verify the calibration result. This verification mainly includes moving distance error measurements as shown in Fig. 13 and repetitive positioning error measurements while maintaining the nominal posture of the robot EE and changing the joint configuration as shown in Fig. 14. A dial gage is fixed on the TX60 EE and a gauge block is fixed on the plane. The dial gage approaches the gauge block and joint angles are recorded as a start point when the dial gage reading reaches a certain value (such as 0.1 mm). Then, the 300-mm long gauge block is removed, the approach motion is repeated, and the joint angles of the end point are recorded. This method can be used to achieve a precise robot movement that is 300 mm long. Note that the line between the start and end points should be as parallel to the gauge block as possible. After calibration, the average error of the motion distance decreased from 2.05 mm to 0.24 mm with 80 mm~440 mm gauge block combinations as the distance reference. The mean error of repetitive positioning, which is the average distance between several points and their average center point, decreased from 1.637 mm to 0.139 mm for different joint configurations.

6. Conclusions

A closed-loop calibration method based on point and distance constraints through machine vision was proposed. The sphere center is taken as the constraint point, and the camera position is adjusted so that the camera optical axis is as close to the sphere center as possible. The point constraint equation is established by taking the sphere center coordinates in the camera coordinate system as the objective function. A gauge block is used as the reference distance. The distance constraint equation is established by using the deviation of the reference distance and calculating the distance as the objective function. The camera is used as a relative position measurement tool and the level of automation of the measurement process is increased. Verification of the calibration result shows that this calibration method improves the absolute positioning accuracy of the robot obviously.

This method has the following advantages. First, the tools used are relatively inexpensive and easy to assemble, disassemble and carry. Second, the high sphericity of the ceramic reference sphere and resolution of the camera ensure high-accuracy measurements. Third, the calibration process can be executed on the robot station without disassembling or transporting the robot, and the space required for calibration is relatively small. Finally, the measurement process is easy to operate.

The calibration methods can still be improved in the following aspects. First, the selection process for sphere position needs to be optimized. Second, the effect of measurement noises on the identification results is difficult to omit.

Declaration of Competing Interest

None.

Acknowledgements

This work was supported by National Natural Science Foundation of China, Grant No.51975157 and Shandong Province Natural Science Foundation, Grant No. ZR2017MEE062.

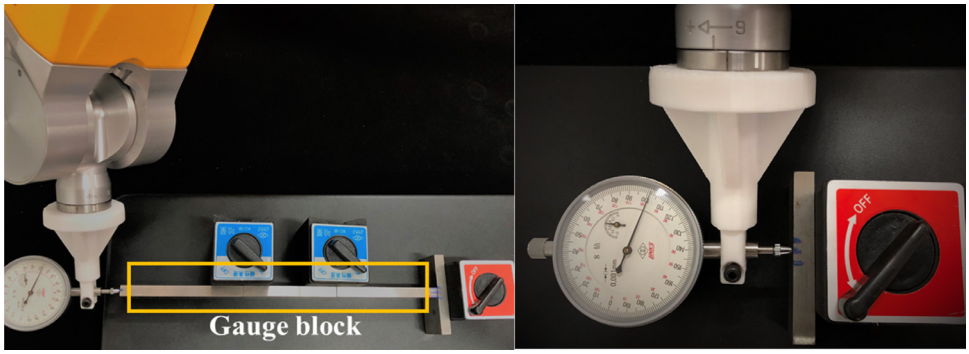

Fig. 13. Detection of robot moving distance errors.

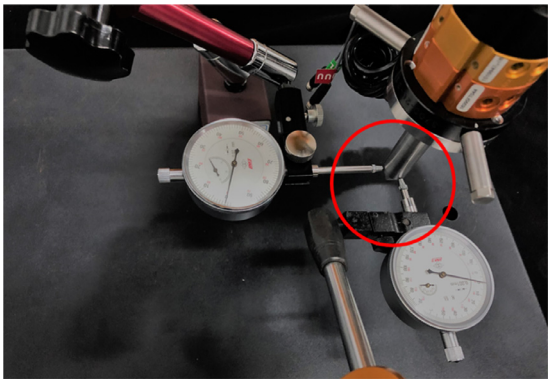

Fig. 14. Detection of robot repetitive positioning errors for different joint configurations.

Reference

[1] Y. Guilin, Applied industrial robotics, Chin. Acad. Sci. 30 (6) (2015) 785–792.
[2] Z. Tie, O. Fan, Task planning and simulation of two-robot welding coordination, Trans. China Weld. Inst. 33 (12) (2012) 9–12+113.
[3] D. Xilun, Z. Lelai, Z. Jun, Pose error analysis of robot in three dimension, J. Beijing Univ. Aeronaut. Astronaut. 35 (2) (2009) 241–245.
[4] H.-.K. Lim, D.-.H. Kim, K. Sung-Rak, et al., ICROS-SICE International Joint Conference, Japan, 2009, p. 2268~2273.
[5] A. Nubiola, I.A. Bonev, Absolute calibration of an ABB IRB 1600 robot using a laser tracker, Robot Comput. Integr. Manuf. 29 (2013) 236–245.
[6] G. Han, Z. Minglu, Z. Xiaojun, et al., Review on key technology of manipulator absolute positioning accuracy calibration, Appl. Res. Comput. 34 (9) (2017) 2570–2576.
[7] G.R. Tang, B.W. Mooring, Plane-motion approach to manipulator calibration, Int. J. Adv. Manuf. Technol. 7 (1) (1992) 21–28.
[8] A. Joubair, I.A. Bonev, Non-kinematic calibration of a six-axis serial robot using planar constraints, Precis. Eng. 40 (2015) 325–333.
[9] G. Du, P. Zhang, Online robot calibration based on vision measurement, Robot. Comput. Integr. Manuf. 29 (2013) 484–492.
[10] . Wang C, Research on the Technique of Robot Autonomous Calibration Based on Vision Assitant Location, Jiangnan University, 2018.
[11] L. Beyer, J. Wulfsberg, Practical robot calibration with Rosy, Robotica 22 (5) (2004) 505–512.
[12] A. Joubair, M. Slamani, I.A. Bonev, kinematic calibration of a five-bar planar parallel robot using allworking modes, Robot Comput. Integr. Manuf. 29 (2013) 15–25.
[13] T. Sun, Y. Zhai, Y. Song, et al., Kinematic calibration of a 3-DoF rotational parallel manipulator using laser tracker, Robot Comput. Integr. Manuf. 41 (2016) 78–91.
[14] G. Legnani, M. Tiboni, Optimal design and application of a low-cost wire-sensor system for the kinematic calibration of industrial manipulators, Mech. Mach. Theory 73 (2014) 25–48.
[15] Y. Lu, Research on Robot Calibration Base on Vision, South China University of Technology, 2013.
[16] Z. Zhao, D. Ye, G. Chen, et al., Binocular vision method of measuring pose based on perpendicular lines, Acta Opt. Sin. 34 (10) (2014) 193–199.
[17] S. Ren, Research of the parallel robot's kinematic calibration and pose tracking based on vision, Harbin Eng. Univ. (2017).
[18] M. Švaco, B. Šekoranja, F. Šuligoj, et al., Calibration of an industrial robot using a stereo vision system, Procedia Eng. (69) (2014) 459–463.
[19] M.R. Driels, U.S. Pathre, Robot manipulator kinematic compensation using a generalized Jacobian formulation, J. Robot. Syst. 4 (2) (1987) 259–280.
[20] M. Grotjahn, M. Daemi, B. HeimaIIll, Friction and rigid body identification of robot dynamics, Int. J. Solids Struct. 38 (10) (2001) 1889–1902.